PHYSICAL REVIEW A VOLUME 12, NUMBER 1 JULY 1975

# Transition to turbulence in a statically stressed fluid system*

John B. McLaughlin† and Paul C. Martin
*Department of Physics, Harvard University, Cambridge, Massachusetts 02138*
(Received 13 January 1975)

A mathematical picture of the transition to turbulence in statically stressed fluid systems is proposed. Systems are classified on the basis of the Hopf bifurcation theorem. One category, "inverted bifurcation," contains flows that exhibit hysteresis, finite-amplitude instabilities, and an immediate transition to turbulent behavior. A mathematical model due to Lorenz which manifests this kind of behavior is discussed. The other category, "normal bifurcation," includes flows in which, as the stress increases, a time-periodic regime precedes turbulence. A model of low-Prandtl-number convection falls into this category. The transition to nonperiodic behavior in this model is studied and found to proceed in accord with abstract mathematical proposals of Ruelle and Takens. Semiquantitative agreement with the experimental fluctuation spectrum of Ahlers is also obtained.

## I. INTRODUCTION

Fluid turbulence remains one of the most fascinating and poorly comprehended phenomena in macroscopic physics. The purpose of this paper is to report on some attempts to understand mathematically how it comes about as the external static stress on a fluid system is increased. We have chosen a statically stressed system to guarantee that the time dependence in the turbulent state arises naturally and is not confused with the effects of internally imposed frequencies. We have been primarily concerned with two questions: how does stochastic time dependence develop as the stress is increased and what is the nature of the fluctuations in the stochastic state?

The commonly accepted picture of the transition to turbulence in statically stressed systems is enunciated by Landau.[1] He pictures the phenomenon as the eventual result of a succession of instabilities at different frequencies. As the stress exceeds each of a sequence of critical stresses, a new unstable, oscillating mode appears in the system. The amplitude of each mode stabilizes at some finite value, which, at least near the critical point, increases monotonically from zero with increasing stress. Turbulence, in this picture, is associated with the complicated state of motion that results when the stress rate is large enough to exceed the thresholds for many instabilities. In keeping with this picture, the motion is quasiperiodic. This behavior is exemplified by a soluble mathematical model due to Hopf.

The Hopf-Landau picture is simply wrong for one class of transitions; for a second, for which it contains an element of truth, it is still deficient in several fundamental ways.

The Hopf-Landau description is least appropriate for the class of flows that exhibit finite amplitude instabilities and hysteresis phenomena. Examples of this class include pipe and channel flow (flow between infinite parallel plates). In the former, there is no linear instability for any finite Reynolds number. In the latter, there is a linear instability at a finite Reynolds number, but there is no periodic regime above the threshold; the transition to a finite degree of turbulence is sudden.

In the second class of flows, there is a periodic regime, in accord with the Hopf-Landau picture. However, strong temporal nonperiodicity sets in after a small number of instabilities have occurred. Thus the frequency spectrum becomes continuous sooner than this picture suggests. It is also observed that the wave-number spectrum stays discrete until higher stresses, where it too becomes continuous. A good qualitative account of this sequence of phenomena for flow past a cylinder can be found in Feynman.[2] The same type of behavior is seen in Couette flow,[3] low-Prandtl-number convection,[4] free shear layers,[5] boundary layers,[6] and the "$n$-layer" models of the earth's atmosphere.[7]

In this paper, a mathematical picture for the transition to nonperiodicity which encompasses and interprets the above flows will be discussed. Specific calculations for examples of the two different types of transitions will be described, and comparisons with the available experiments will be made. The two sets of calculations were performed for a model of thermal convection in an infinite fluid layer in two different regimes of Prandtl number (the ratio of kinematic viscosity to thermal diffusivity). In the high-Prandtl-number regime, an example of an inverted bifurcation is obtained; in the low-Prandtl-number regime, a normal bifurcation is found. In both cases, the transition to nonperiodicity and the behavior of the nonperiodic orbits are studied.

## II. GENERAL THEORY OF THE TRANSITION TO TURBULENCE

We have indicated that there are two categories of turbulent systems, those that show abrupt transitons and those that exhibit a periodic regime, and that the difference between them can be interpreted on the basis of the Hopf bifurcation theorem.[8] Let us be slightly more specific. The Hopf bifurcation theorem states that, in the neighborhood of the stress at which a complex-conjugate pair of roots of the linear stability problem cross the real frequency axis, there is a one-parameter family of limit-cycle solutions. Ruelle and Takens[8] and, independently, Joseph and Sattinger[9] have shown that this theorem is valid for the equations of fluid mechanics.

If the limit cycle occurs for values of the stress smaller than the value at the point of neutral stability the point will be called an "inverted bifurcation." In this case, the limit cycle is unstable, if the system is released at a point in phase space inside the limit cycle, it spirals into the laminar state. If a system is released outside the limit cycle, it spirals away from the limit cycle into other regions of phase space.

As the stress on the system is increased, the unstable limit cycle shrinks at the point of neutral stability. Above threshold, the limit cycle disappears, and in the known examples the system immediately spirals out and enters a strongly nonperiodic orbit. In the example to be discussed in Sec. IV, this nonperiodic orbit maps out an invariant surface in the phase space of the system. This invariant surface is an example of a "strange attractor."[8] It is possible that in the other examples of inverted bifurcation in fluid mechanics the nonperiodic orbits may also lie on strange attractors in the appropriate phase spaces.

Pipe flow provides a possible exception to the above classification. The problem with pipe flow is associated with the fact that its linear threshold lies at infinite stress. It turns out that the real frequency axis contains a dense set of accumulation points for the eigenvalues of the linear stability problem. Thus, even in the linear theory, there is a continuous frequency spectrum at the point of neutral stability. This fact makes it difficult, if not impossible, to apply the arguments that have been used to establish the Hopf bifurcation theorem in other examples, since an infinite-dimensional phase space must be considered. While in pipe flow an unstable limit cycle might not coalesce with the laminar state at the point of neutral stability, this picture does apply to flow in a pipe containing a coaxial wire, since in this case the system has a linear threshold at a finite Reynolds number.

The second category of flows consists of those flows that have a one-parameter family of limit-cycle solutions above the linear threshold in stress. For this class, the limit cycle is stable and the flow is periodic for a range of Reynolds numbers. The question of how these flows become nonperiodic has been attached by Ruelle and Takens[8] using mathematical methods devised by Smale[10] and others. The basic idea is to study the "generic" behavior of integral curves in appropriate phase spaces. They do so by showing that for dense open sets of vector fields in the phase space certain types of behavior "usually occur" among all loosely constrained differential transformations ("diffeomorphisms") which map the vector fields into one another. Application of these results to the particular diffeomorphism described by the Navier-Stokes equations are predicated on the assumption that the Navier-Stokes equations are "typical" and not "special." Ruelle and Takens claim to show that after four bifurcations have occurred a certain broad class of diffeomorphisms will produce an open set of vector fields with a strange attractor in the neighborhood of every point in a certain physically interesting region of the phase space. If they are correct, the Hopf model which violates their picture must be "nongeneric."

Before discussing the above idea in more detail, it is necessary to explain what is meant by "$n$" bifurcations. At low values of the external stress, the laminar state of a fluid system is linearly stable. When the stress is increased through the linear threshold, a limit cycle bifurcates from the laminar state. If the external stress is increased further, it will eventually reach the value at which the next pair of complex-conjugate eigenvalues of the linear theory cross the real frequency axis. Of course, these eigenvalues no longer have meaning in general since it is necessary to study the stability of the limit cycle itself and not the laminar state. However, if the amplitude of the limit cycle happens to be very small at the second threshold, the stability analysis of the higher-lying degrees of freedom should be approximately the same as if the first instability had not occurred. If this is the case, the limit cycle will become unstable to a new solution at the second threshold. This new solution bifurcates from the limit cycle and, in general, moves away in function space from it. More generally it is expected that a solution, limit cycle or otherwise, will become unstable to solutions in which the amplitudes of higher-lying degrees of freedom increase in size. In practice, it is quite difficult to establish the location of higher-order bifurcations. Their location

is signaled by an anomalously rapid growth in the amplitude of new degrees of freedom.

The situation after two and three bifurcations have occurred is rather nebulous. Reulle and Takens claim that the motion after two bifurcations should still generically be periodic. They base this claim on a theorem due to Peixoto.[10] We do not understand their argument (more specifically, how to reconcile it with the Hopf model, which gives rise to almost periodic attractors), but some steps in their argument may have escaped us.

The situation after three bifurcations is even less clear than after two bifurcations. It appears than any number of possibilities could occur, and none seem more likely than any of the others. Ruelle and Takens only claim to have shown that the vector fields are generically not Morse-Smale after three bifurcations. A field which is Morse-Smale has a nonwandering set[8] which consists of a finite number of fixed points and closed orbits.

After four bifurcations have occurred, Ruelle and Takens argue that the motion should generically lie on a strange attractor. This means that the motion should be nonperiodic and that correlation functions of the dynamical variables should go to zero as the time separation between the variables goes to infinity. Such motions are termed "pseudorandom" in the mathematical literature. In this paper, they will be referred to simply as "nonperiodic."

The above ideas are supported by the calculations reported in Sec. V. These calculations exhibit the surprising feature that the motion remains strictly periodic after three bifurcations, but becomes nonperiodic after the fourth. This same behavior is found in the experiments discussed in Sec. V.

## III. EXPERIMENTAL AND MATHEMATICAL BACKGROUND OF THERMAL CONVECTION

### A. Experimental background

The phenomenon of thermal convection occurs when the buoyancy force in a fluid due to externally imposed temperature gradients exceeds external frictional forces and the internal dissipative forces of the fluid. The buoyancy force occurs in most fluids because they expand when heated. Because of this expansion, the light hot fluid will rise and the heavy cold fluid will fall in an external gravitational field.

In order to study the phenomenon of thermal convection, it is common to impose a temperature difference across a thin layer of fluid. If the fluid layer is thin enough that variation in material properties of the fluid with height can be ignored and large enough to avoid certain complicated effects due to boundaries, the convection pattern takes the form of two-dimensional rolls.[11] Lord Rayleigh[12] first studied this phenomenon theoretically and calculated the temperature difference at which the rolls would form.

As the temperature difference across the layer is increased, the convective motion becomes faster, and eventually time dependence develops. The experiments of Willis and Deardorff[4] indicate that the behavior of the fluid in the time-dependent regime depends qualitatively on the ratio of the kinematic viscosity $\nu$ to the thermal diffusivity $\kappa$. The ratio $\sigma$ is called the Prandtl number

$$\sigma \equiv \nu/\kappa . \tag{3.1}$$

Willis and Deardorff performed one set of experiments on air, for which $\sigma = 0.71$. They found that an oscillatory time dependence developed when the temperature difference was roughly three times the convective threshold. More specifically, the wavy convection rolls exhibited lateral oscillations which appeared to be closely in phase and relatively constant in amplitude everywhere but near the surface of the fluid layer. This observation suggests that the undulations are insensitive to boundaries and that calculations in which, for simplicity, the fluid is assumed to have free surfaces may not be grossly misleading. The first calculations of small oscillations of convective rolls in low-Prandtl-number fluids, were performed by Busse,[13] who employed this approximation. He found an instability that resulted in long-wavelength oscillations of the rolls. The extension of his analysis to account for nonlinear effects is contained in Sec. V.

Willis and Deardorff have also performed experiments with a silicone oil for which $\sigma = 57$. Time dependence did not develop in it until the temperature difference exceeded 60 times that at the convective threshold. As in air the time dependence above threshold was oscillatory, but, in contrast with air, the oscillatory structure was not a roll but "an up or down draft segment having one end anchored to a more prominent up or down draft and the other end free."

Krishnamurti[14,15] has also conducted experiments on fluids with a wide range of Prandtl number. In air, her results agree closely with those of Willis and Deardorff. In mercury, a highly conducting (low Prandtl-number) fluid, she observed a somewhat higher threshold than that predicted by Busse's stability analysis. By contrast Rossby[16] found, in agreement with Busse's predictions, that time dependence developed in mercury immediately above the convective threshold. The agreement between Rossby's experiments and Busse's

theory may be illusory. Rossby's observations were made less slowly than Krishnamurti's, and he may have been misled by transient effects. If her experiments are correct, it seems likely that the disagreement between theory and experiment may have to be laid to the use of inappropriate boundary conditions in the stability analysis.

Krishnamurti's experiments on water, for which $\sigma = 6.7$, and on fluids with larger Prandtl numbers showed that in these fluids the time dependence was associated with plumes which broke off from the thermal boundary layer at the low surface. These rising plumes seemed similar in character to those observed by Willis and Deardorff in silicone oil.

Unpublished calculations by Gough, Spiegel, and Toomre[17] are reported to have reproduced the oscillatory behavior in high-Prandtl-number flows. These calculations entail the extensive vertical resolution necessary to adequately represent the thermal boundary layers and the interactions for plume formation. The horizontal variation is represented by a simple plan-form in which all horizontal harmonics are dropped. The complementary calculations with greater horizontal resolution and less vertical resolution seem more appropriate for low-Prandtl-number fluids.

In Sec. IV we will examine a greatly oversimplified model of convection which yields a transition to time dependence in large-Prandtl-number fluids. Since it lacks the vertical resolution necessary to reproduce the plumes discussed above, it is not realistic. We include it because it is mathematically interesting; it provides an example of inverted bifurcation. The model, a triad of Fourier components coupled through the Boussinesq equations, can serve as a useful guide in thinking about hysteresis, metastability, and other phenomena it has in common with real fluid systems that undergo inverted bifurcation.

### B. Mathematical background

In order to obtain a tractable mathematical problem, it is customary to model a real convection layer which is bounded on all sides by an infinite fluid layer which has free surfaces and to assume that the fluid satisfies the Boussinesq conditions, that the material properties of the fluid do not vary appreciably with height and that the heat generated by internal friction in the fluid is negligible. Finally, the motions involved in experiments on convection layers are always extremely small compared with the speed of sound so that the fluids may be considered incompressible.

It can be shown[18] that incompressible fluids which obey the Boussinesq conditions obey the equations

$$\frac{\partial u_i}{\partial t} + u_j \frac{\partial u_i}{\partial x_j} = g\epsilon \Delta T \delta_{i3} - \frac{1}{\rho}\frac{\partial P}{\partial x_i} + \nu \nabla^2 u_i \,,$$

$$\frac{\partial T}{\partial t} + u_j \frac{\partial T}{\partial x_j} = \kappa \nabla^2 T \,, \tag{3.2}$$

$$\frac{\partial u_i}{\partial x_i} = 0 \,.$$

In Eqs. (3.2), $u_i$ is the $i$th component of velocity, $x_i$ is the $i$th spatial coordinate ($i = 3$ being the vertical coordinate), $t$ is the time, $g$ is the gravitational constant, $\epsilon$ is the coefficient of thermal expansion, $\Delta T$ is the difference between the temperature at a given point and the average temperature of the fluid layer, $\rho$ is the density of the fluid, $T$ is the temperature and $P$ the pressure of the fluid at a given point and time, and $\kappa$ is the coefficient of thermal diffusivity.

If there is no motion in the fluid layer, the solutions of Eq. (3.2) yield $u = 0$ and the characteristic linear conduction temperature profile between the two surfaces of the layer. It is useful to take this fact into account by introducing a new temperature variable $\theta$,

$$\Delta T(x_1, x_2, x_3, T) = \overline{T} - \Delta T_0 (x_3/H) + \theta(x_1, x_2, x_3, T) \,. \tag{3.3}$$

In this definition, $\overline{T}$ is a constant which is determined by requiring conservation of mass, $\Delta T_0$ is the difference between the temperatures of the two surfaces, and $H$ is the thickness of the fluid layer.

It is also convenient to introduce dimensionless variables

$$\begin{aligned} &x_i \to x_i H \,, \qquad t \to t H^2/\kappa \,, \\ &u_i \to u_i \kappa/H \,, \quad \theta \to \Theta \kappa \nu / g\epsilon H^3 \,. \end{aligned} \tag{3.4}$$

Equations (3.4) can be used to reduce Eqs. (3.2) to the form

$$\frac{\partial u_i}{\partial t} + u_j \frac{\partial u_i}{\partial x_j} - \delta_{i3}\sigma\left(\overline{T} - \frac{\Delta T_0}{H} x_3 + \theta\right) + \frac{1}{\rho}\frac{\partial P}{\partial x_i} - \sigma \nabla^2 u_i = 0 \,,$$

$$\frac{\partial \theta}{\partial t} + u_j \frac{\partial \theta}{\partial x_j} - R u_3 - \nabla^2 \theta = 0 \,, \tag{3.5}$$

where $\sigma = \nu/\kappa$ is the Prandtl number, and $R$, the Rayleigh number, is defined by

$$R \equiv g\epsilon H^3 \nabla T_0 / \kappa \nu \,. \tag{3.6}$$

Equations (3.5) can be reduced to a system of coupled nonlinear equations by introducing Fourier series for the fields. These discrete Fourier series involve well-defined fundamental wavelengths in the horizontal directions. There are also solutions of the Boussinesq equations which

involve continuous wave-number spectra. However, calculations to be reported elsewhere indicate that, in the case of the system discussed in Sec. V, the stable solutions involve continuous wave-number distributions which are sharply peaked around well-defined wavelengths. This will be taken to be an experimentally observed fact in this paper. Thus the following discrete spectra will be assumed:

$$u_i = i \sum_{l,m,n=-\infty} u_i(l,m,n) e^{i(k_1 l x + k_2 m y + n\pi z)} ,$$

$$\theta = i \sum_{l,m,n=-\infty} \theta(l,m,n) e^{i(k_1 l x + k_2 m y + n\pi z)} . \tag{3.7}$$

The coordinates $(x, y, z)$ are $(x_1, x_2, x_3)$ and $k_1$ and $k_2$ are the dimensionless fundamental wave numbers in the $x$ and $y$ directions. Likewise the components of velocity $(u, v, w)$ are $(u_1, u_2, u_3)$.

Substituting (3.7) into Eqs. (3.5) and eliminating the pressure term by the incompressibility condition, we find

$$\frac{du_{lmn}}{dt} = -\sum_{pqr}\left[k_1\left(\frac{lr-pn}{n-r}+lA_{lmnpr}\right)u_{pqr}u_{l-p,m-q,n-r} + \left(-k_2\frac{nq-mr}{n-r}+k_1 lB_{lmnpqr}\right)u_{pqr}v_{l-p,m-q,n-r}\right.$$
$$\left. + k_1 l C_{lmnqr} v_{pqr} v_{l-p,m-q,n-r}\right] - \sigma(k_1^2 l^2 + k_2^2 m^2 + \pi^2 n^2) u_{lmn} - \frac{k_1 \pi\sigma \ln\theta_{lmn}}{k_1^2 l^2 + k_2^2 m^2 + \pi^2 n^2} , \tag{3.8a}$$

$$\frac{dv_{lmn}}{dt} = -\sum_{pqr}\left[k_2 m A_{lmnpr} u_{pqr} u_{l-p,m-q,n-r} + \left(\frac{k_1}{r}(-lr+np) + mk_2 B_{lmnpqr}\right)u_{pqr}v_{l-p,m-q,n-r}\right.$$
$$\left. + k_2\left(\frac{mr-nq}{n-r}+mC_{lmnqr}\right)v_{pqr}v_{l-p,m-q,n-r}\right] - \sigma(k_1^2 l^2 + k_2^2 m^2 + \pi^2 n^2) v_{lmn} - \frac{k_2 \pi\sigma mn\theta_{lmn}}{k_1^2 l^2 + k_2^2 m^2 + \pi^2 n^2} , \tag{3.8b}$$

$$\frac{d\theta_{lmn}}{dt} = -\sum_{pqr}\left[\left(\frac{k_1}{r}(pn-lr)u_{pqr} + \frac{k_2}{r}(qn-mr)v_{pqr}\right)\theta_{l-p,m-q,n-r}\right] - (k_1^2 l^2 + k_2^2 m^2 + \pi^2 n^2)\theta_{lmn} - R(k_1 l u_{lmn} + k_2 m v_{lmn}) , \tag{3.8c}$$

with

$$A_{lmnpr} \equiv \frac{k_1^2(np-lr)(nl-lr+np)}{(k_1^2 l^2 + k_2^2 m^2 + \pi^2 n^2)(n-r)r} ,$$
$$B_{lmnpqr} \equiv \frac{2k_1 k_2 (mr-qn)(pn-lr)}{(k_1^2 l^2 + k_2^2 m^2 + \pi^2 n^2)(n-r)r} , \tag{3.9}$$
$$C_{lmnqr} \equiv \frac{k_2^2 (mr-nq)(nq-mr-mn)}{(k_1^2 l^2 + k_2^2 m^2 + \pi^2 n^2)(n-r)r} .$$

Equations (3.8) constitute an infinite set of coupled nonlinear differential equations for the modes of the system. As a preliminary to concrete calculations, it is useful to eliminate some modes by symmetry arguments. First, it is clear from Eqs. (3.8) that the modes can be taken to be real. These solutions correspond to the choice of standing waves instead of traveling waves. This choice is somewhat arbitrary since Willis and Deardorff reported seeing both traveling and standing waves in their experiments on air.

Equations (3.7) imply that for the modes to be real and the velocity and temperature fields to be real, the relations

$$u_{lmn} = -u_{-l,-m,-n} ,$$
$$v_{lmn} = -v_{-l,-m,-n} , \tag{3.10}$$
$$\theta_{lmn} = -\theta_{-l,-m,-n} ,$$

must be satisfield.

As boundary conditions we shall assume that the vertical component of velocity and temperature deviation $\theta$ vanish at the two surfaces. In view of the incompressibility, these conditions become

$$\theta = \frac{\partial}{\partial z}\left(\frac{\partial u}{\partial x} + \frac{\partial v}{\partial y}\right) = 0 \quad \text{at } z = 0, H . \tag{3.11}$$

Equations (3.7) and (3.11) imply that

$$u_{lmn} = u_{l,m,-n} ,$$
$$v_{lmn} = v_{l,m,-n} , \tag{3.12}$$
$$\theta_{lmn} = -\theta_{l,m,-n} .$$

Equations (3.10) and (3.12) imply that certain modes vanish:

$$u_{00n} = v_{00n} = \theta_{lm0} = 0 . \tag{3.13}$$

The solutions of Eqs. (3.8) can be broken into even and odd parts on the basis of whether they are even or odd under $l \to -l$. The symmetry of a given mode can then be determined by using Eqs. (3.10) and (3.12). This decomposition is used in Sec. V.

In order to make comparisons with experiments, the total heat flux through the fluid layer can be expressed in terms of the temperature modes. Let us denote an average over horizontal coordinates

by angular brackets. The horizontal average of Eq. (3.2),

$$\frac{\partial\langle T\rangle}{\partial t}+\left\langle u_j\frac{\partial T}{\partial x_j}\right\rangle=\kappa\nabla^2 T\,,$$

can be simplified by integrating by parts and using the incompressibility condition,

$$\frac{\partial\langle T\rangle}{\partial t}+\frac{\partial}{\partial z}\left(\langle wT\rangle-\kappa\frac{\partial\langle T\rangle}{\partial z}\right)=0\,.$$

From this equation we obtain for the vertical heat transfer $J$

$$J=\langle wT\rangle-\kappa\frac{\partial\langle T\rangle}{\partial z}\,. \tag{3.14}$$

If the convection layer is statistically steady, $\langle T\rangle$ has no time dependence and

$$\partial J/\partial z=0\,, \tag{3.15}$$

which implies that the flux leaving the lower surface is the same as that reaching the upper surface. Since the vertical component of velocity vanishes at both surfaces, Eq. (3.14) yields

$$J=-\kappa\frac{\partial\langle T\rangle}{\partial z}(z=0)\,;$$

or, with the heat flux expressed in terms of the deviation from the conduction profile according to Eqs. (3.3) and (3.4),

$$\begin{aligned}J&=\frac{\kappa\Delta T_0}{H}-\frac{\kappa^2\nu}{g\epsilon H^3}\left(\frac{\partial\langle\theta\rangle}{\partial z}\right)_{z=0}\\&=\frac{\kappa^2\nu}{g\epsilon H^3}\left[R-\left(\frac{\partial\langle\theta\rangle}{\partial z}\right)_{z=0}\right].\end{aligned} \tag{3.16}$$

An expression for $J$ in terms of the modes of the system is obtained by inserting Eq. (3.7) into Eq. (3.16),

$$J=\frac{\kappa^2\nu}{g\epsilon H^3}\left(R+2\pi\sum_{n=1}^{\infty}n\theta_{00n}\right)\,. \tag{3.17}$$

It is sometimes useful to introduce a dimensionless number called the Nusselt number $N$ which expresses the ratio of the total heat flux to the heat transported by conduction. According to (3.17) the Nusselt number is given by

$$N=1+\frac{2\pi}{R}\sum_{n=1}^{\infty}n\theta_{00n}\,. \tag{3.18}$$

## IV. INVERTED BIFURCATION–THE LORENZ MODEL

### A. Model

The solutions to Eqs. (3.8) have received much attention. It is well known, for example, that a transition to convective motion in the form of two dimensional rolls occurs at a critical Rayleigh number $R_c$ and the amplitude of the convective motion grows continuously from zero as the Rayleigh number is increased above threshold. The solution to Eqs. (3.8) can be calculated perturbatively when the amplitude of the motion is small. To second order in the amplitude, only three modes are nonzero.[13] These modes are $u_{101}$, $\theta_{101}$, and $\theta_{002}$ (with the roll motion chosen to lie in the $x$-$z$ plane).

In this section, a model system consisting of $u_{101}$, $\theta_{101}$, and $\theta_{002}$ will be studied at Rayleigh numbers at which the model no longer applies to fluids. At these Rayleigh numbers the model exhibits a transition to time-dependent behavior which has interesting mathematical properties even though it does not apply to actual fluid convection. In the model there is an inverted bifurcation, and beyond the point of bifurcation the system point tends towards a "strange attractor" in its phase space. Since the system has the same type of nonlinearity, driving, and dissipation as the full Boussinesq equations, it bolsters the proposal of Ruelle and Takens[8] that strange attractors are relevant in real fluid systems.

As is apparent from Eq. (3.17), the heat flux may be described entirely in terms of modes which have zero wave numbers in the $x$ and $y$ directions. We shall call these modes transport modes and label them with a subscript $T$. We shall also introduce the transformations and definitions

$$\begin{aligned}&u\to -u(\pi^2+k_1^2)/2^{3/2}k_1\,, && \theta\to\theta(\pi^2+k_1^2)^3/2^{3/2}\pi k_1^2\,,\\&v\to -v(\pi^2+k_1^2)/2^{3/2}k_1\,, && \theta_T\to\theta_T(\pi^2+k_1^2)^3/2\pi k_1^2\,,\\&t\to t/(\pi^2+k_1^2)\,, && R_c\equiv(\pi^2+k_1^2)^3/k_1^2\,,\\&r\equiv R/R_c\,, && b\equiv 4\pi^2/(\pi^2+k_1^2)\,.\end{aligned} \tag{4.1}$$

Substituting the three modes described above into Eqs. (3.8) and making use of the transformations and definitions in Eqs. (4.1), we find

$$\begin{aligned}\dot u_{101}&=\sigma\theta_{101}-\sigma u_{101}\,,\\\dot\theta_{101}&=-u_{101}\theta_{002}+ru_{101}-\theta_{101}\,,\\\dot\theta_{002}&=u_{101}\theta_{101}-b\theta_{002}\,.\end{aligned} \tag{4.2}$$

These equations were first studied by Lorenz,[19] who denoted $u_{101}$, $\theta_{101}$, and $\theta_{002}$ by $x$, $y$, and $z$, respectively. Lorenz's notation will be used henceforth in order to avoid subscripts.

There are three steady-state solutions to Eqs. (4.2). One is the trivial solution in which all three variables vanish, i.e.,

$$x=y=z=0\,. \tag{4.3}$$

This solution corresponds to conduction; the fluid layer is at rest and the temperature profile between the two surfaces is linear.

The other two steady-state solutions are given by

$$x = y = \pm[b(r-1)]^{1/2} \equiv \pm c\,, \quad z = r-1\,. \tag{4.4}$$

The two solutions (4.4) correspond to a simple roll plan-form in which the velocity field and horizontal dependence of the temperature deviation from the conduction profile is described by $x$ and $y$, respectively. The horizontally averaged distortion of the temperature profile from that of the conducting state is given by $z$. The variables $x$, $y$, $z$ and their relationship to observable quantities are shown in Fig. 1.

### B. Linear stability analysis

The two solutions in Eqs. (4.4) will be called "laminar" solutions since they correspond to a steady motion of the fluid. In order to study the stability of the laminar solutions, it is useful to study the perturbations

$$\begin{aligned} \delta x &\equiv x - [b(r-1)]^{1/2}\,, \\ \delta y &\equiv y - [b(r-1)]^{1/2}\,, \\ \delta z &\equiv z - (r-1)\,. \end{aligned} \tag{4.5}$$

Linearizing Eqs. (4.3) around the positive solution of Eqs. (4.4), we obtain, for the perturbations introduced in (4.5), the equations

$$\begin{aligned} \delta\dot{x} &= -\sigma(\delta x - \delta y)\,, \\ \delta\dot{y} &= \delta x - \delta y - [b(r-1)]^{1/2}\delta z\,, \\ \delta\dot{z} &= [b(r-1)]^{1/2}\delta x + [b(r-1)]^{1/2}\delta y - b\,\delta z\,. \end{aligned} \tag{4.6}$$

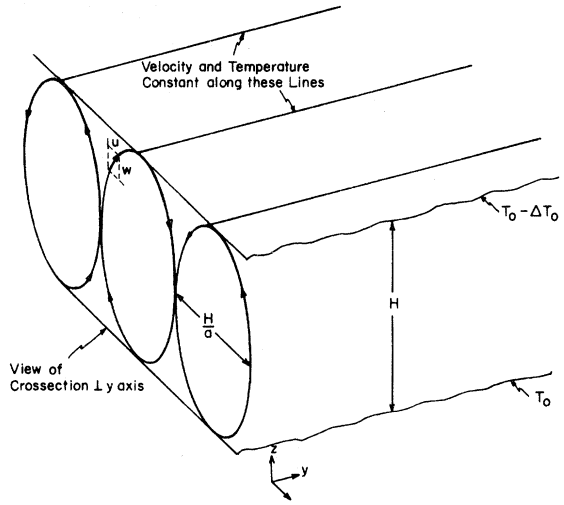


$$u = -\sqrt{2}\,\pi\kappa\,\frac{(1+a^2)}{a} \times \sin\left(\frac{\pi a x}{H}\right)\cos\left(\frac{\pi z}{H}\right)$$

$$W = \sqrt{2}\,\pi\kappa\,(1+a^2) \times \cos\left(\frac{\pi a x}{H}\right)\sin\left(\frac{\pi z}{H}\right)$$

$$T = T_0 - \frac{\Delta T_0}{H}\,z + \frac{\kappa\nu}{g\alpha H^2}\,\frac{\pi^3(1+a^2)^3}{a^2}\left(\sqrt{2}\;Y\cos\left(\frac{\pi a x}{H}\right)\sin\left(\frac{\pi z}{H}\right) - Z\sin\left(\frac{2\pi z}{H}\right)\right)$$

FIG. 1. Velocity and temperature fields in roll plan form for the Lorenz model.

The stability of these is studied, as usual, by introducing

$$\delta x(t) = \delta x e^{\lambda t} \tag{4.7}$$

and similar equations for $\delta y(t)$ and $\delta z(t)$. When these expressions are inserted in Eqs. (4.6) and $\delta x$, $\delta y$, and $\delta z$ are eliminated, a cubic secular equation is obtained:

$$\lambda^3 + (\sigma + b + 1)\lambda^2 + b(r+\sigma)\lambda + 2\sigma b(r-1) = 0\,. \tag{4.8}$$

Equation (4.8) has one real negative root and two complex-conjugate roots when $r$ is greater than one. The two complex-conjugate roots have a negative real part when $r$ is less than a certain value $r_T$. For these values of $r$, infinitesimal perturbations to the laminar state will decay in time. At $r_T$, the two complex conjugate roots cross the imaginary axis. When $r > r_T$, perturbations to the laminar state grow with time, that is, the laminar state becomes unstable. The value of $r_T$ is determined by demanding that the complex conjugate roots be pure imaginary:

$$(\lambda + i\lambda_0)(\lambda - i\lambda_0)(\lambda - \lambda_1) = \lambda^3 - \lambda_1\lambda^2 + \lambda_0^2\lambda - \lambda_1\lambda_0^2 = 0\,. \tag{4.9}$$

We see from Eq. (4.9) that $r_T$ may be determined by requiring that the product of the coefficients of $\lambda$ and $\lambda^2$ equal the constant term in Eq. (4.8), or that

$$(\sigma + b + 1)b(r_T + \sigma) = 2\sigma b(r_T - 1)\,.$$

We therefore have

$$r_T = \sigma(\sigma + b + 3)/(\sigma - b - 1)\,. \tag{4.10}$$

Note that $r_T$ goes to infinity as $\sigma$ approaches $b+1$; for $\sigma < b+1$ there is no solution. Since, by definition, $b$ must lie between 0 and 4, this threshold does not exist for small values of the Prandtl number. Thus, for example, the Lorenz model gives rise to a time-independent roll plan form at all Rayleigh numbers for air for which $\sigma = 0.71$. This conclusion seems related to and consistent with the studies of Willis and Deardorff.[20] They have argued, on the basis of experiments in which three-dimensional behavior was inhibited by adjusting a pair of styrofoam buffers, that time dependence in air flows is always preceded by the development of a three-dimensional pattern. They have also numerically integrated the two-dimensional Boussinesq equations for air to test this hypothesis. These numerical studies indicated that the laminar state was stable for all values of the Rayleigh number examined, apart from a curious pulsation of the cells which they attribute to the boundary conditions they used.

### C. Numerical solutions

Lorenz[19] has integrated Eqs. (4.2) on a machine for values of $r$ which exceed $r_T$. His calculations were performed for $\sigma = 10$ and $b = \frac{8}{3}$. This value of $b$ corresponds to $k_1^2 = \frac{1}{2}\pi^2$, which is the critical value of $k_1$ deduced by Lord Rayleigh.[11] With these values of $\sigma$ and $b$, $r_T = 24.74$; Lorenz studied the solutions with $r = 28$.

Lorenz found that the system spiralled away from each of the two laminar solutions in the phase space of the three modes, and that it spiralled back and forth about the two laminar points indefinitely. The deterministic orbits he calculated exhibit several interesting features. The first and perhaps most unexpected feature is the nonperiodicity of the orbits in time. The system point rotates about one center for two or three orbits, and then moves off to rotate about the other center for a series of orbits. There is no apparent relation regularity in the number of orbits about either of the two centers.

Lorenz mapped out the region of phase space that was occupied by the nonperiodic orbits described above. This region is a doubly connected infinitely-many-sheeted surface in the phase space, which we shall henceforth refer to as the "Lorenz surface." The projection of the Lorenz surface onto the $y$-$z$ plane is shown in Fig. 2.

The movement of a system on the Lorenz surface can be qualitatively described as follows. Assuming that a system is initially close to one of the two laminar points and on the upper (lower) branch of the surface for the plus (minus) center, it spirals steadily outward from the center until its radius attains a critical value. When the system attains the critical radius, it crosses over to an orbit about the other center before it can complete another revolution about the first center. In describing this crossing-over process, let us suppose, for definiteness, that the system is spiralling out from the plus center. It strikes the critical radius and describes a trajectory near the upper (in $z$) edge of the Lorenz surface as it approaches the minus center. The system then winds around the minus center and comes down onto the lower (in $x$) branch of the Lorenz surface, circling underneath the branch that it came in on. In the next stage, the system spirals out from the minus center until it again reaches the critical radius and comes in toward the plus center from below on the lower branch. The system then swings up around the plus center onto the upper branch. At this point, the system is back in the general location where it started and repeats the whole characteristic but irregular process *ad infinitum*.

It is clear that the dimensionality of the phase space is crucial in the process described above. It is difficult to imagine such nonperiodic orbits in a one- or two-dimensional system having the same type of nonlinearity, damping, and static driving as Eqs. (4.2); when a system moves in towards a center, there is no way for it to escape from the center. In one dimension, the system would have to retrace its path, and this is impossible for a first order differential equation in which the time derivative of a variable depends only on the variable. In two dimensions, it would appear that all orbits must be either periodic or asymptotically periodic.

The Lorenz surface appears to be one of the simplest possible examples of the "strange-attractor" solutions discussed by Ruelle and Takens.[8] In fact, the Lorenz surface bears a strong resemblance to one of the examples of a strange attractor that was given by Ruelle and Takens. This example is a structure that is embedded in a three-dimensional space and which is locally the product of a Cantor set and a piece of two-dimensional surface. The attractor thus has measure zero in the phase space, and is an infinitely-many-sheeted surface.

Probably the most important consequence of the nonperiodicity discussed above is the possibility of doing statistical mechanics without introducing external stochastic elements into the basic equations. Numerical calculations of the correlation functions of the three modes indicate that they phase mix to zero in roughly one rotation period. Ruelle and Takens point out that mixing behavior

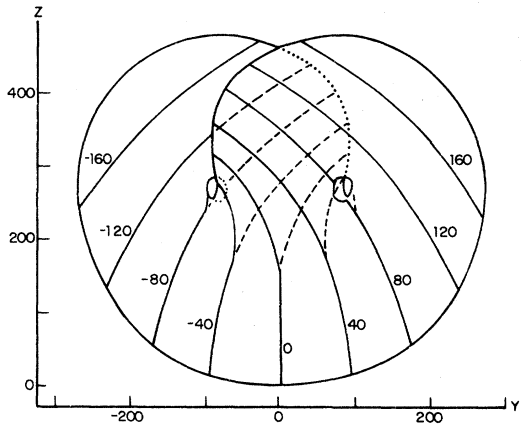


FIG. 2. Isopleths of $x$ as a function of $y$ and $z$ (thin solid curves) and isopleths of the lower of two values of $x$, where two values occur (dashed curves), for approximate surfaces formed by all points on limiting trajectories. Heavy solid curve, and extensions as dotted curves, indicate natural boundaries of surfaces. (Reprinted by permission of E. N. Lorenz.)

should be obtained for systems with strange attractors.

### D. Landau expansion

To show that the Lorenz model is an example of inverted bifurcation, we shall make a Landau expansion, that is, an expansion in the amplitude of the deviation of the orbit from one of the laminar points.

From Eqs. (4.6)–(4.8), it is easily seen that, at $r_T$, an infinitesimal perturbation to the plus center has an infinite lifetime and enters an orbit about the center:

$$\begin{aligned}
&\delta x_0 = A\cos(\omega_T t)\,,\\
&\delta y_0 = A[\cos(\omega_T t) - (\omega_T/\sigma)\sin(\omega_T t)]\,,\\
&\delta z_0 = (A\omega_T/\sigma c_0)[\omega_T\cos(\omega_T t) + (\sigma+1)\sin(\omega_T t)]\,,
\end{aligned} \tag{4.11}$$

with

$$c_0^2 \equiv b(r_T - 1), \quad \omega_T^2 \equiv 2\sigma b(\sigma+1)/(\sigma - b - 1)\,, \tag{4.12}$$

and $A$ an arbitrary infinitesimal real number. Let us first consider values of $r$ slightly less than $r_T$. The corrections to the orbit given in Eqs. (4.11) can be calculated perturbatively by setting

$$\delta x = \delta x_l + \delta x_{nl}\,, \tag{4.13}$$

and similarly for $\delta y$ and $\delta z$. The subscript "$l$" denotes the part of the system's coordinates which can be found from linear theory while "$nl$" denotes the nonlinear correction to the orbit. If $r$ is close to $r_T$, we can take

$$\delta x_l = \delta x_0, \quad \delta y_l = \delta y_0, \quad \delta z_l = \delta z_0\,. \tag{4.14}$$

This replacement constitutes the lowest approximation in a perturbation expansion in the quantity $\Delta c$,

$$\Delta c \equiv [b(r-1)]^{1/2} - [b(r_T - 1)]^{1/2}\,. \tag{4.15}$$

Inserting Eqs. (4.5) and (4.15) into Eqs. (4.2) we obtain

$$\begin{aligned}
&\delta\dot{x} = -\sigma(\delta x - \delta y)\,,\\
&\delta\dot{y} = \delta x - \delta y - c_0\delta z - \delta x\delta z - \Delta c\,\delta z\,,\\
&\delta\dot{z} = c_0\delta x + c_0\delta y - b\,\delta y + \delta x\delta y + \Delta c\,\delta x + \Delta c\,\delta y\,.
\end{aligned} \tag{4.16}$$

We next insert Eqs. (4.13) into Eqs. (4.16) and equate terms of first order in the nonlinearity:

$$\begin{aligned}
&\delta\dot{x}_{nl} = -\sigma(\delta x_{nl} - \delta y_{nl})\\
&\delta\dot{y}_{nl} = \delta x_{nl} - \delta y_{nl} - c_0\delta z_{nl} - \delta x_l\delta z_l - \Delta c\,\delta z_{nl}\\
&\delta\dot{x}_{nl} = c_0\delta x_{nl} + c_0\delta y_{nl} - b\,\delta z_{nl} + \delta x_l\delta y_l\\
&\qquad + \Delta c\,\delta x_{nl} + \Delta c\,\delta y_{nl}\,.
\end{aligned} \tag{4.17}$$

For values of $r$ close to $r_T$, we need only keep terms of zero order in $\Delta c$ in Eqs. (4.17). Making use of Eqs. (4.11), (4.14), and (4.17), we find

$$\begin{aligned}
&\delta\dot{x}_{nl} = -\sigma(\delta x_{nl} - \delta y_{nl})\,,\\
&\delta\dot{y}_{nl} = \delta x_{nl} - \delta y_{nl} - c_0\delta z_{nl}\\
&\qquad - (A^2\omega_T/2\sigma c_0)\{\omega_T[1+\cos(2\omega_T t)]\\
&\qquad\qquad + (\sigma+1)\sin(2\omega_T t)\}\,,\\
&\delta\dot{z}_{nl} = c_0\delta x_{nl} + c_0\delta y_{nl} - b\,\delta z_{nl}\\
&\qquad + (A^2/2\sigma)\{\sigma[1+\cos(2\omega_T t)]\\
&\qquad\qquad - \omega_T\sin(2\omega_T t)\}\,.
\end{aligned} \tag{4.18}$$

Equation (4.18) can be satisfied by $\delta x_{nl}$, $\delta y_{nl}$, and $\delta z_{nl}$, which have the following form:

$$\begin{aligned}
&\delta x_{nl} = B\cos(2\omega_T t) + C\sin(2\omega_T t) + D\,,\\
&\delta y_{nl} = E\cos(2\omega_T t) + F\sin(2\omega_T t) + G\,,\\
&\delta z_{nl} = H\cos(2\omega_T t) + I\sin(2\omega_T t) + J\,.
\end{aligned} \tag{4.19}$$

A system of nine inhomogeneous linear equations for the nine unknowns $B$–$J$ is generated by substituting (4.19) into (4.18) and equating the coefficients of the orthogonal functions:

$$\begin{aligned}
&2\omega_T B = \sigma(C - F)\,,\\
&2\omega_T C = -\sigma(B - E)\,,\\
&D = G\,,\\
&-2\omega_T E = C - F - c_0 I - (\sigma+1)\omega_T A^2/2\sigma c_0\,,\\
&2\omega_T F = B - E - c_0 H - \omega_T^2 A^2/2\sigma c_0\,,\\
&0 = -c_0 J - \omega_T^2 A^2/2\sigma c_0\,,\\
&-2\omega_T H = c_0 C + c_0 F - bI - \omega_T A^2/2\sigma\,,\\
&2\omega_T I = c_0 B + c_0 E - bH + A^2/2\,,\\
&0 = c_0 D + c_0 G - bJ + A^2/2\,.
\end{aligned} \tag{4.20}$$

A straightforward but lengthy calculation yields

$$\begin{aligned}
&B = \beta A^2\,,\\
&C = (\alpha\beta+\gamma)A^2\,,\\
&D = G = -[1 + (b\omega_T^2/\sigma c_0^2)](A^2/4c_0)\,,\\
&E = [\beta + \gamma + (2\omega_T\alpha\beta/\sigma)]A^2\,,\\
&F = [\alpha + \gamma - (2\omega_T/\sigma)]A^2\,,\\
&H = [\omega_T(8\beta c_0 - 1) - 4(\sigma+1)(\alpha\beta+\gamma)c_0](\omega_T A^2/2\sigma c_0^2),\\
&I = [8\omega_T(\alpha\beta+\gamma)c_0 + (\sigma+1)(4\beta c_0 - 1)](\omega_T A^2/2\sigma c_0^2)\,,\\
&J = -\omega_T^2 A^2/2\sigma c_0^2\,,
\end{aligned} \tag{4.21}$$

where the parameters $\alpha$, $\beta$, and $\gamma$ are defined by the equations

$$\alpha = \frac{3\omega_T^2}{2\omega_T^2(\sigma + b + 1) - \sigma c_0^2}\,,$$

$$\beta=\frac{\omega_T^2(2\sigma+2+b)+\sigma c_0^2-12\omega_T^3 c_0}{4c_0[2\omega_T^2(\sigma+b+1)+3\alpha\omega_T^3-\sigma c_0^2]}, \qquad (4.22)$$

$$\gamma=\frac{2\omega_T b(\sigma+1)-3\omega_T^3}{4c_0[2\omega_T^2(\sigma+b+1)-\sigma c_0^2]}.$$

Near the transition point $r_T$, the growth or decay of an infinitesimal perturbation to the laminar state should be small. Thus it is useful to introduce the growth rate averaged over one period, $2\pi/\omega_T$. From Eq. (4.16) we see that to first order in the nonlinearity and $\Delta c$

$$X\equiv\frac{1}{2}\frac{d}{dt}\langle(\delta x^2+\delta y^2+\delta z^2)\rangle$$
$$=-\sigma\langle\delta x_{nl}^2\rangle-\langle\delta y_{nl}^2\rangle-b\langle\delta z_{nl}^2\rangle$$
$$+(\sigma+1)\langle\delta x_{nl}\delta y_{nl}\rangle+c_0\langle\delta x_{nl}\delta z_{nl}\rangle+\Delta c\langle\delta x_0\delta z_0\rangle, \qquad (4.23)$$

with the angular brackets indicating an average over one period. The growth rate can be expressed in terms of $A,\ldots,J$ by substituting (4.11) and (4.19) into (4.23). We have

$$2X=-\sigma(B^2+C^2+2D^2)-(E^2+F^2+2G^2)$$
$$-b(H^2+I^2+2J^2)+(\sigma+1)(BE+CF+2DG)$$
$$+c_0(EH+FI+2GJ)+(A^2\omega_T^2\Delta c/\sigma c_0). \qquad (4.24)$$

Inserting the solutions (4.21), we obtain

$$2X=-\sigma(B^2+C^2-BE-CF)-(E^2+F^2-BE-CF)$$
$$-b(H^2+I^2)+c_0(EH+FI)+A^2\omega_T^2\Delta c/\sigma c_0$$
$$+(A^4\omega_T^2/4\sigma^2c_0^2)[\sigma-\omega_T^2(r_T-1)^{-1}]. \qquad (4.25)$$

From (4.11) we also have

$$2X=[1+\omega_T^2(c_0^2+\sigma^2+2\sigma+2)/2\sigma c_0^2](dA^2/dt). \qquad (4.26)$$

Equations (4.21) and (4.22) and (4.25) and (4.26) can be used to calculate the growth rate. To simplify the algebra let us consider high-Prandtl-number flows and expand all quantities in the inverse of the Prandtl number. The quantities $r_T$ and $\omega_T$ given by (4.10) and (4.12) become

$$r_T=\frac{\sigma(\sigma+b+3)}{\sigma-b-1}, \qquad (4.27)$$
$$\omega_T=\left[\frac{2\sigma b(\sigma+1)}{\sigma-b-1}\right]^{1/2}.$$

The quantities $c_0$, $\alpha$, $\beta$, and $\gamma$ can also be expanded in powers of $\sigma^{-1}$. From (4.12), (4.22), and (4.27) we obtain

$$c_0=(b\sigma)^{1/2}[1+(2b+3)/2\sigma],$$
$$\alpha=(8b/\sigma)^{1/2}[1+b/2\sigma], \qquad (4.28)$$
$$\beta=(\sigma b)^{-1/2}(5/12)[1+(15-62b)/10\sigma],$$
$$\gamma=-(\sqrt{2}/3\sigma)[1-3(b+1)/2\sigma].$$

From (4.27) and (4.28) we obtain expressions for $B-J$ and the last two terms in Eq. (4.25) in terms of $b$ and $\sigma$. Furthermore, to order $\sigma^{-1}$, Eq. (4.26) simplifies to $X=\frac{1}{2}dA^2/dt$. With these replacements (4.25) finally becomes

$$\frac{dA^2}{dt}=\frac{37}{72\sigma}A^4+\left(\frac{b}{\sigma}\right)^{1/2}\Delta cA^2. \qquad (4.29)$$

Equation (4.29) has the form with which Landau begins his discussion with a crucial exception: the sign of the $A^4$ term is positive, not negative. The quantity $\Delta c$ is positive when $r$ is greater than $r_T$ and negative when $r$ is less than $r_T$. Thus, when $r$ is less than $r_T$, we may infer the existence of an unstable limit cycle. Then the Lorenz model exhibits inverted bifurcation.

The limit cycle occurs for that value of $A$ which makes the growth rate identically zero. Denoting this value of $A$ by $A_c$, we find from Eq. (4.29)

$$A_c=(72\,|\Delta c\,|/37)^{1/2}(b\sigma)^{1/4}. \qquad (4.30)$$

For values of $A$ larger than $A_c$, the system will spiral away from the laminar point. For values of $A$ less than $A_c$, a system will be pulled into the laminar state.

The perturbation expansion in $A$ is only reliable if $A$ is substantially less than one. Since, to lowest order in the $1/\sigma$ expansion, the $\Delta c=(r_T-r)/2c_0$, this condition is equivalent to

$$r_T-r\ll 1. \qquad (4.31)$$

Numerical calculations reveal that the $1/\sigma$ expansion breaks down for values of $\sigma$ larger than 10, the value used by Lorenz. For accurate results one must use the values of $\omega_T$, $c_0$, $\alpha$, $\beta$, and $\gamma$ given by Eqs. (4.12) and (4.22) and compute the growth rate with Eqs. (4.21) and (4.25). With the values used by Lorenz, $\sigma=10$ and $b=\frac{8}{3}$, the expression for $A_c$ becomes

$$A_c=24.4\,|\Delta c\,|^{1/2}. \qquad (4.32)$$

For this equation to hold it is necessary that $|\Delta c|\ll 1.67\times10^{-3}$, whence from (4.15)

$$r_T-r\ll 0.01. \qquad (4.33)$$

For larger values of $r_T-r$, Eq. (4.32) overestimates $A_c$, the neglected terms in the Landau expansion drive the system outward and decrease $A_c$.

Since the $A^2$ expansion of the growth rate breaks down for $A^2$ greater than 1, the existence of an unstable limit cycle cannot be inferred in this region. However, it is easy to see if the limit cycle remains and measure its size. Such a calculation reveals that as $r$ decreases, for $b=\frac{8}{3}$ and $\sigma=10$, the limit cycle steadily increases in size until $r$ reaches 21. At this point, it becomes impossible to find orbit-type solutions about the two cen-

ters. The phase space is divided into two parts. One part is in the domain of attraction of one center and the other is in the domain of attraction of the other center.

Thus, in the region $21 < r < 24.74$, finite amplitude instabilities exist. If a system is released outside one of the limit cycles, it spirals away from it and then proceeds to execute the usual motions on the Lorenz surface which were discussed in Sec. IV C. It might be thought that the unstable limit cycles surrounding the two laminar points would prevent the system from becoming trapped by one of the two laminar points. This is not the case. The limit cycles are on the upper sheets for the plus center and the lower sheets for the minus center. Thus, there is nothing on the "approach sheets" to prevent the system from being pulled into one of the laminar points. If a system spiralling away from the plus center comes close enough to the edge of the Lorenz surface, it will execute a tight swing down around the minus center into the domain of attraction of the minus center on the lower sheets.

The essential ingredients in the above behavior are the center-manifold theorem,[8] the three dimensionality of the phase space, and the nonlinearity of the equations of motion. The center-manifold theorem implies that orbits near either of the two laminar points should be attracted onto a two-dimensional surface (the center manifold). The nonlinearity of the equation of motion drives the system far away from a laminar point if the system is released outside the unstable limit cycle on the center manifold. However, the three-dimensionality of the phase space allows the system to come back to the laminar point from a direction outside the center manifold. Since this direction is not in the center manifold, the system is pulled into the center manifold and either trapped by the laminar point or recycled depending on whether it lands inside or outside the unstable limit cycle.

Thus the Lorenz model provides one of the simplest possible examples of metastability and hysteresis. It is hoped that it may prove helpful in gaining insight into more realistic examples of such phenomena in pipe and channel flow.

## V. NORMAL BIFURCATION–LOW-PRANDTL-NUMBER CONVECTION

### A. Linear theory

The Lorenz model of convection discussed in Sec. IV fails to predict any time dependence in low-Prandtl-number convection. Busse[13] has found the linear instability which leads to time dependence in such flows. The instability involves a wave motion along the length of the convection rolls, which has been observed in experiments on air by Willis and Deardorff.[4] Coles[3] has seen similar wave motion of the Taylor cells in his Couette flow experiments.

The basic mechanism responsible for the time dependence in low-Prandtl-number convection is a shear instability. The shear, or velocity gradient, which produces the instability has its maximum value at the points where the fluid is rising or falling most rapidly. At these points the $x$ component of velocity (see Fig. 1) vanishes. We therefore expect the $x$ component of the wave velocity to behave like $\cos(kx)$ if the $x$ component of the roll velocity is $\sin(kx)$.

Busse approximated the basic convection rolls by the three Lorenz modes $u_{101}$, $T_{101}$, and $T_{002}$. This can be justified in the limit of zero Prandtl number since the amplitudes of all other modes vanish as higher powers of the Prandtl number. More generally, Busse showed that the three-mode truncation is valid whenever the amplitude of the convection is small.

Consider the system of modes which have the correct symmetry to couple to the roll gradients and which satisfy the following conditions:

$$\begin{aligned} &|l| \leq 1, \quad |n| \leq 2, \\ &|m| = 1, \quad |l| + |n| \leq 2 \text{ and even}. \end{aligned} \tag{5.1}$$

The modes which satisfy these conditions are $u^0_{111}$, $v^e_{111}$, $u_{010}$, $u_{012}$, and $\theta^0_{111}$. Busse found that this truncation for the wave modes leads to errors of about 20% in the growth rate.

The five modes discussed above and the three roll modes constitute a system of 8 modes. Substituting these modes into Eqs. (3.6) and employing Eqs. (4.1), we obtain

$$\frac{du_{101}}{dt} = \frac{u_{111}u_{010}}{\sqrt{2}} + \frac{(3-a_1^2)u_{111}u_{012}}{(1+a_1^2)\sqrt{2}} - \frac{a_2(I-a_1^2)}{a_1(1+a_1^2)} \frac{(u_{010}v_{111} - u_{012}v_{111})}{\sqrt{2}} + \sigma(\theta_{101} - u_{101}), \tag{5.2a}$$

$$\frac{du_{111}}{dt} = -\frac{u_{101}u_{010}}{2\sqrt{2}} - \frac{(3-a_1^2)u_{101}u_{012}}{(1+a_1^2)2\sqrt{2}} + \frac{\sigma(1+a_1^2)\theta_{111}}{1+a_1^2+a_2^2} - \frac{\sigma(1+a_1^2+a_2^2)u_{111}}{1+a_1^2}, \tag{5.2b}$$

$$\frac{dv_{111}}{dt} = \frac{\sqrt{2}a_1a_2}{1+a_1^2+a_2^2} u_{101}u_{012} + \frac{\sigma a_2(1+a_1^2)}{a_1(1+a_1^2+a_2^2)} \theta_{111} - \frac{\sigma(1+a_1+a_2^2)}{1+a_1^2} v_{111}, \tag{5.2c}$$

$$\frac{du_{010}}{dt}=\frac{\sqrt{2}a_2}{a_1}u_{101}v_{111}-\frac{\sigma a_2^2}{1+a_1^2}u_{010}, \tag{5.2d}$$

$$\frac{du_{012}}{dt}=-\frac{a_2}{\sqrt{2}a_1}u_{101}v_{111}-\frac{\sigma(4+a_2^2)}{1+a_1^2}u_{012}, \tag{5.2e}$$

$$\frac{d\theta_{101}}{dt}=\frac{u_{010}\theta_{111}}{\sqrt{2}}-\frac{u_{012}\theta_{111}}{\sqrt{2}}-u_{101}\theta_{002}+ru_{101}-\theta_{101}, \tag{5.2f}$$

$$\frac{d\theta_{002}}{dt}=2u_{111}\theta_{111}+\frac{2a_2v_{111}\theta_{111}}{a_1}+u_{101}\theta_{101}-\frac{4\theta_{002}}{1+a_1^2}, \tag{5.2g}$$

$$\frac{d\theta_{111}}{dt}=-u_{111}\theta_{002}-\frac{u_{010}\theta_{101}}{2\sqrt{2}}+\frac{u_{012}\theta_{101}}{2\sqrt{2}}-\frac{a_2v_{111}\theta_{002}}{a_1}+ru_{111}+\frac{ra_2v_{111}}{a_1}-\frac{(1+a_1^2+a_2^2)\theta_{111}}{1+a_1^2}, \tag{5.2h}$$

with $a_1\equiv k_1/\pi$ and $a_2=k_2/\pi$. Since no ambiguity exists the superscripts on $u^e_{111}$, $v^0_{111}$, and $\theta^0_{111}$ have been deleted in Eqs. (5.2). Note that Eqs. (5.2) reduce to Eqs. (4.2) when $u_{111}$, $v_{111}$, $u_{010}$, $u_{012}$, and $\theta_{111}$ are set equal to zero. Thus the straight convection roll is a solution to Eqs. (5.2) and it is stable for sufficiently small values of $r$.

If Eqs. (5.2) are linearized around the roll solution given by Eqs. (4.2), a system of five equations is obtained:

$$\begin{aligned}
&\left(\lambda+\frac{\sigma(1+a_1^2+a_2^2)}{1+a_1^2}\right)u_{111}=-\frac{cu_{010}}{2\sqrt{2}}-\left(3-\frac{4a_1^2}{1+a_1^2+a_2^2}\right)\frac{cu_{012}}{2\sqrt{2}}+\frac{\sigma(1+a_1^2)\theta_{111}}{1+a_1^2+a_2^2},\\
&\left(\lambda+\frac{\sigma(1+a_1^2+a_2^2)}{1+a_1^2}\right)v_{111}=\frac{\sqrt{2}a_1a_2cu_{012}}{1+a_1^2+a_2^2}+\frac{\sigma a_2(1+a)\theta_{111}}{a_1(1+a_1^2+a_2^2)},\\
&\left(\lambda+\frac{\sigma a_2^2}{1+a_1^2}\right)u_{010}=\frac{\sqrt{2}a_2cv_{111}}{a_1},\\
&\left(\lambda+\frac{\sigma(4+a_2^2)}{1+a_1^2}\right)u_{012}=-\frac{a_2cv_{111}}{\sqrt{2}a_1},\\
&\left(\lambda+\frac{(1+a_1^2+a_2^2)}{1+a_1^2}\right)\theta_{111}=u_{111}+\frac{a_2v_{111}}{a_1}-\frac{c(u_{010}-u_{012})}{2\sqrt{2}}.
\end{aligned} \tag{5.3}$$

The eigenvalues and eigenfunctions of Eqs. (5.3) can be calculated by making a perturbation expansion in $a_2$. That is to say, the wavelength in the $y$ direction may be assumed to be much larger than the thickness of the layer, and an expansion will be made in the ratio of these wavelengths carried out.

Let us choose $u_{111}$ to be unity. To zeroth order in $a_2$, we obtain one condition:

$$\theta^{(0)}_{111}=1. \tag{5.4}$$

To first order, three more conditions appear:

$$v^{(1)}_{111}=1/a_1;\quad \theta^{(1)}_{111}=0;\quad \lambda^{(1)}=-(c/2\sqrt{2})u^{(1)}_{010}. \tag{5.5}$$

In second order, the eigenvalue is determined to first order:

$$\begin{aligned}
&u^{(2)}_{012}=-c(1+a_1^2)/4\sqrt{2}\sigma a_1^2,\\
&u^{(1)}_{010}=\mp i2/a_1,\\
&v^{(2)}_{111}=\mp ic/\sqrt{2}a_1^2\sigma,\\
&\theta^{(2)}_{111}=\frac{1}{(\sigma+1)}\left(\frac{2\sigma}{1+a_1^2}+\frac{1}{a_1^2(1+a_1^2)}-\frac{c^2}{4\sigma a_1^2}\right),\\
&\lambda^{(1)}=\pm ic/\sqrt{2}a_1,\\
&\lambda^{(2)}=\theta^{(2)}_{111}-\frac{cu^{(2)}_{012}}{2\sqrt{2}}+\frac{1}{a_1^2(1+a_1^2)}-\frac{c^2(1+a_1^2)}{16\sigma a_1^2}.
\end{aligned} \tag{5.6}$$

Finally, when terms of third order in $a_2$ are considered, the eigenvalue is determined to second order:

$$\lambda^{(2)}=-\frac{\sigma}{(\sigma+1)(1+a_1^2)}+\frac{\sigma}{2a_1^2(\sigma+1)(1+a_1^2)}-\frac{\sigma}{2(1+a_1^2)}+\frac{c^2}{4\sigma a_1^2}\left(1+\frac{1}{2(\sigma+1)}-\frac{(1+a_1^2)}{8}\right). \tag{5.7}$$

From (5.6) and (5.7) it follows that, to first order in $a_2$, the eigenfrequency is pure imaginary, and to second order, it is real. The point of neutral stability occurs when the real part of the eigenfrequency vanishes. Equation (5.7) gives for neutral stability the condition

$$c^2=\tfrac{32}{3}\sigma^2(\sigma+1)/(13\sigma+21), \tag{5.8}$$

which corresponds to a Rayleigh number

$$r_T=1+4\sigma^2(\sigma+1)/(13\sigma+21). \tag{5.9}$$

This threshold is actually valid only in the limit of infinite wavelength, since it was obtained by making an expansion in $a_2$. Finite wavelengths are more strongly damped, and therefore the threshold for finite wavelengths is higher than that in Eq. (5.9).

### B. Landau expansion

The Landau expansion for Eqs. (5.2) is obtained by the same procedures used in Sec. IV. To set up the expansion, we introduce the notation

$$\begin{aligned}
\delta u_{101}&=a^{(0)}_{101}A^2e^{(\lambda+\lambda^*)t}+a^{(2)}_{101}A^2e^{2\lambda t}+a^{(2)*}_{101}A^2e^{2\lambda^* t}+O(A^4),\\
\delta u_{111}&=A(e^{\lambda t}+e^{\lambda^* t}),\\
\delta v_{111}&=a_{111}Ae^{\lambda t}+\alpha^{(0)}_{111}A^3e^{(2\lambda+\lambda^*)t}+\alpha^{(3)}_{111}A^3e^{3\lambda t}+\text{c.c.}+O(A^6),
\end{aligned}$$

$$\delta u_{010} = a_{010}Ae^{\lambda t} + \alpha^{(0)}_{010}A^3e^{(2\lambda+\lambda^*)t} + \alpha^{(3)}_{010}A^3e^{3\lambda t} + \text{c.c.} + O(A^6),$$

$$\delta u_{012} = a_{012}Ae^{\lambda t} + \alpha^{(0)}_{012}A^3e^{(2\lambda+\lambda^*)t} + \alpha^{(3)}_{012}A^3e^{3\lambda t} + \text{c.c.} + O(A^6),$$

$$\delta T_{101} = b^{(0)}_{101}A^2e^{(\lambda+\lambda^*)t} + b^{(2)}_{101}A^2e^{2\lambda t} + b^{(2)*}_{101}A^2e^{2\lambda^* t} + O(A^4),$$

$$\delta T_{002} = b^{(0)}_{002}A^2e^{(\lambda+\lambda^*)t} + b^{(2)}_{002}A^2e^{2\lambda t} + b^{(2)*}_{002}A^2e^{2\lambda^* t} + O(A^4),$$

$$\delta T_{111} = b_{111}Ae^{\lambda t} + \beta^{(0)}_{111}A^3e^{(2\lambda+\lambda^*)t} + \beta^{(3)}_{111}A^3e^{3\lambda t} + \text{c.c.} + O(A^6), \tag{5.10}$$

From Eqs. (5.2) and (5.10) it follows that when $r = r_T$, so that the linear growth rate vanishes, the real part of $\lambda$ is of order $A^2$. Furthermore, the real part of the growth rate can be incorporated into the definition of $A^2$. As a result, we may write

$$\frac{dA^2}{dt} = \alpha A^2 + \beta A^4. \tag{5.11}$$

In order to calculate the quantity $\beta$, we shall assume that $r$ is set equal to $r_T$. Thus the nonlinear contribution to the growth rate will be calculated to zeroth order in $r - r_T$.

To second order in $A$, the quantities $a^{(0)}_{101}$, $a^{(2)}_{101}$, $b^{(0)}_{101}$, $b^{(2)}_{101}$, $b^{(0)}_{002}$, and $b^{(2)}_{002}$ are nonzero. These quantities can be calculated from Eqs. (5.2a), (5.2f), and (5.2g) by expanding in $a_2$. To zeroth order in $a_2$, the modes have the values

$$a^{(0)}_{101} = b^{(0)}_{101} = -2/c_0; \quad b^{(0)}_{002} = 0, \qquad a^{(2)}_{101} = b^{(2)}_{101} = -1/c_0; \quad b^{(2)}_{002} = 0. \tag{5.12}$$

The variable $c_0$ is the value of $c$ for $r = r_T$. To first order in $a_2$ all three modes vanish. To second order in $a_2$ only the modes $b^{(0)}_{002}$ and $b^{(2)}_{002}$ will be needed to calculate $\beta$:

$$b^{(0)}_{002}(2) = \frac{1}{c_0}\left[\left(\frac{\sigma+1}{\sigma}\right)\left(\frac{4\sigma}{c(1+a_1^2)} - \frac{2c}{a_1^2\sigma}\right) - \frac{c(1+a_1^2)}{4\sigma^2a_1^2}\left(3 - \frac{4a_1^2}{1+a_1^2} - \sigma\right)\right]. \tag{5.13}$$

Denoting the part of the eigenfrequency which is second order in $A$ by $\lambda_2$, we find, from Eqs. (5.2) to third order in $A$, the system of equations

$$\lambda_2 = -\frac{\sqrt{2}}{4}(a^{(0)}_{101}a_{010} + a^{(2)}_{101}a^*_{010} + c\,\alpha^{(1)}_{010}) - \sqrt{2}\left(\frac{3}{4} - \frac{a_1^2}{1+a_1^2+a_2^2}\right)(a^{(0)}_{101}a_{012} + a^{(2)}_{101}a^*_{012} + c\,\alpha^{(1)}_{012}) + \frac{\sigma(1+a_1^2)\beta^{(1)}_{111}}{1+a_1^2+a_2^2},$$

$$\lambda_2 a_{111} + i\omega\alpha^{(1)}_{111} = \frac{\sqrt{2}a_1a_2}{1+a_1^2+a_2^2}(a^{(0)}_{101}a_{012} + a^{(2)}_{101}a^*_{012} + c\,\alpha^{(1)}_{012}) + \frac{\sigma a_2(1+a_1^2)\beta^{(1)}_{111}}{a_1(1+a_1^2+a_2^2)} - \frac{\sigma(1+a_1^2+a_2^2)\alpha^{(1)}_{111}}{1+a_1^2},$$

$$\lambda_2 a_{010} + i\omega\alpha^{(1)}_{010} = \frac{\sqrt{2}a_2}{a_1}(a^{(0)}_{101}a_{111} + a^{(2)}_{101}a^*_{111} + c\,\alpha^{(1)}_{111}) - \frac{\sigma a_2^2\alpha^{(1)}_{010}}{1+a_1^2},$$

$$\lambda_2 a_{012} + i\omega\alpha^{(1)}_{012} = -\frac{a_2}{\sqrt{2}a_1}(a^{(0)}_{101}a_{111} + a^{(2)}_{101}a^*_{111} + c\,\alpha^{(1)}_{111}) - \frac{\sigma(4+a^2)\alpha^{(1)}_{012}}{(1+a_1^2)},$$

$$\lambda_2 b_{111} + i\omega\beta^{(1)}_{111} = -\frac{1}{2\sqrt{2}}(a^{(0)}_{101}a_{010} + a^{(2)}_{101}a^*_{010} + c\,\alpha^{(1)}_{010} + \frac{1}{2\sqrt{2}}(a^{(0)}_{101}a_{012} + a^{(2)}_{101}a^*_{012} + c\,\alpha^{(1)}_{012}) + \frac{a_2\alpha^{(1)}_{111}}{a_1} - b^{(0)}_{002} - b^{(2)}_{002} - \frac{a_2a_{111}b^{(0)}_{002}}{a_1} - \frac{a_2a^*_{111}b^{(2)}_{002}}{a_1} - \frac{(1+a_1^2+a_2^2)\beta^{(1)}_{111}}{1+a_1^2}. \tag{5.14}$$

We can solve (5.14) by expanding in powers of $a_2$. To zeroth order all powers vanish. To first order we have

$$\alpha^{(1)}_{010}(1) = 2i/c^2a_1, \quad \lambda_2(1) = -i\sqrt{2}/ca_1, \tag{5.15}$$

and to second order

$$\alpha^{(1)}_{111}(2) = \sqrt{2}i/\sigma ca_1^2,$$

$$\alpha^{(1)}_{010}(2) = \frac{2\sqrt{2}}{c}\lambda_2(2) + \frac{2\sqrt{2}\sigma}{c^3(1+a_1^2)} + \frac{\sqrt{2}}{c\sigma a_1^2},$$

$$\alpha^{(1)}_{012}(2) = 3\sqrt{2}(1+a_1^2)/8\sigma ca_1^2,$$

$$\lambda_2(2) = -(5\sigma+13)/8\sigma(\sigma+1). \tag{5.16}$$

Since $\beta$ is equal to twice the real part of $\lambda_2$, we have

$$\beta = -a_2^2(5\sigma+13)/4\sigma(\sigma+1). \tag{5.17}$$

The variable $\alpha$ can be determined from Eq. (5.7):

$$\alpha = \frac{(r-r_T)}{\sigma a_1^2(1+a_1^2)}\left(1 + \frac{1}{2(\sigma+1)} - \frac{(1+a_1^2)}{8}\right). \tag{5.18}$$

Equations (5.11), (5.17), and (5.18) show that bifurcation resulting from Eqs. (5.2) is a normal bifurcation.

For high Prandtl numbers, the normal bifurcation is shorted out by the inverted bifurcation, dis-

cussed in Sec. IV, since the threshold for the Lorenz instability, given by Eq. (4.10), grows like $\sigma$ for large $\sigma$, while the instability discussed in this section [as can be seen from Eq. (5.9)] grows as $\sigma^2$. The actual crossing point of the instabilities occurs for $\sigma$ near 10. Numerical calculations for larger Prandtl numbers reveal that the three Lorenz modes execute their usual nonperiodic motion while the other five modes go to zero.

### C. Evolution of nonperiodicity

The work in Sec. V B showed that the model of low-Prandtl-number convection studied in this section provides an example of normal bifurcation. Thus the ideas presented in Sec. II and the proposal of Ruelle and Takens that four bifurcations are generically needed to produce nonperiodic motion can be tested. For this purpose we may include four wave numbers $(k_y, 2k_y, 3k_y, 4k_y)$ in the $y$ direction and determine by numerical integration whether the motion becomes nonperiodic. Note that we can adjust all four bifurcations to occur arbitrarily close to the threshold given in Eq. (5.9) by choosing $k_y$ small enough. Thus conditions which are arbitrarily close to those assumed by Ruelle and Takens can be created.

The lowest consistent truncation which has four harmonics in the $y$ direction is defined by the conditions

$$\begin{aligned} &|l| \leq 1, \quad |m| \leq 4, \\ &|n| \leq 2, \quad |l| + |n| \leq 2 \text{ and even}. \end{aligned} \tag{5.19}$$

The truncation contains 39 modes: first, there is the roll mode, $u_{101}$, and four other modes, $u^0_{111}$, $u^0_{121}$, $u^0_{131}$, and $u^0_{141}$, which have the same symmetry as $u_{101}$ and nonvanishing wave numbers in the $y$ direction. Although these modes have the opposite symmetry from those which are linearly unstable, they play an important role in the dynamics because of the nonlinear terms in the Navier-Stokes equation. For small $k_y$, they are only slightly more damped than the roll mode and they can have comparable magnitudes.

The five temperature modes which correspond to these velocity modes are $\theta_{101}$, $\theta^e_{111}$, $\theta^e_{121}$, $\theta^e_{131}$, and $\theta^e_{141}$. Each of these temperature modes is found to be closely phase-locked to its corresponding velocity mode.

There are also four modes associated with $\theta_{002}$. These modes are $\theta_{012}$, $\theta_{022}$, $\theta_{032}$, and $\theta_{042}$. The four new modes remain very small compared to $\theta_{002}$ in all the calculations. There is a good physical reason for this behavior. The mode $\theta_{002}$ is the only transport mode in the model. If the modes $\theta_{012}$, $\theta_{022}$, $\theta_{032}$, and $\theta_{042}$ were to drain off a sizeable fraction of the amplitude of the $\theta_{002}$ mode, there would be a decrease in the convective heat transport. To take a limiting case, suppose that the periodic boundary conditions along the $y$ direction were allowed to recede to infinity so that a whole band of wave numbers were allowed. In that limit, the convective heat transport would go to zero if all modes $\theta_{0k2}$ were on an equal basis with $\theta_{002}$. This result is not seen experimentally.

It is necessary to include the modes $v^e_{111}$, $v^e_{121}$, $v^e_{131}$, and $v^e_{141}$ because of the nonlinearity of the equations of motion.

The rest of the modes are harmonics of the linearly unstable set of modes studied in this section. Thus there are five sets of four modes: $u^e_{111}$, $u^e_{121}$, $u^e_{131}$, $u^e_{141}$, $v^0_{111}$, $v^0_{121}$, $v^0_{131}$, $v^0_{141}$, $u_{010}$, $u_{020}$, $u_{030}$, $u_{040}$, $u_{012}$, $u_{022}$, $u_{032}$, $u_{042}$, $\theta^0_{111}$, $\theta^0_{121}$, $\theta^0_{131}$, $\theta^0_{141}$.

The equations for the 39 modes are found by substituting them into Eqs. (3.8) and dropping couplings to higher-lying modes.

In the actual calculations we wish to report, $a_2$ was chosen to be $0.1a_1$, or 0.072, and Prandtl number was chosen to be unity. These choices were made so that the results could be compared with the results of Ahlers's experiments on convection

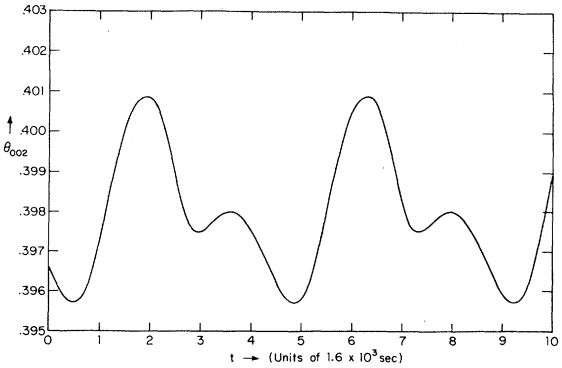


FIG. 3. $\theta_{002}$ vs $t$ for $r=1.4$, 4 wavelengths.

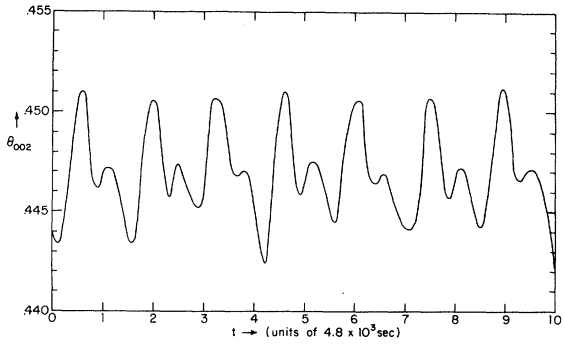


FIG. 4. $\theta_{002}$ vs $t$ for $r=1.45$, 4 wavelengths.

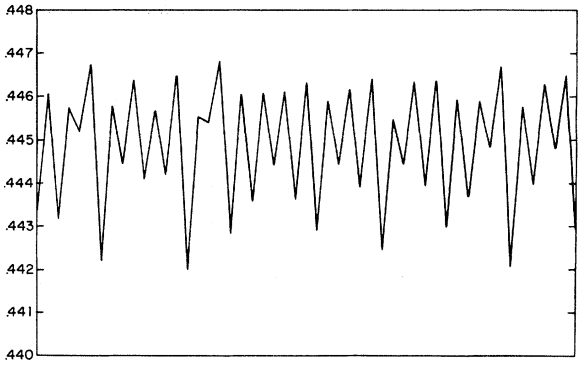


FIG. 5. Minima of $\theta_{002}$ for $r=1.45$, 4 wavelengths.

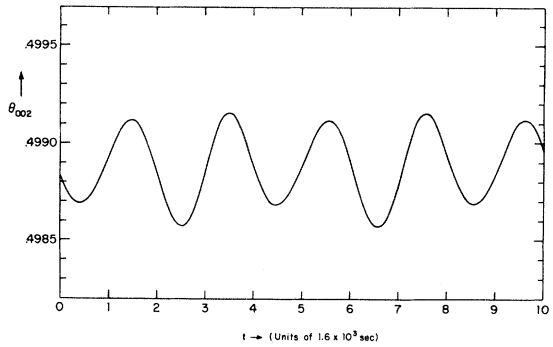


FIG. 7. $\theta_{002}$ vs $t$ for $r=1.5$, 4 wavelengths.

in classical helium at low temperatures. Ahlers did his experiments in a cylindrical geometry. However, for the purpose of rough comparison, the ratio of the plate separation to the circumference of the plates multiplied by 2 yields a value of 0.086 for $a_2$. The Prandtl number of the helium that Ahlers used was 0.86.

Ahlers found a sharp transition to nonperiodic fluctuations of about 1% in the heat flux at $r=2.18$. He did not see any periodic regime, but this may be due to the fact that the heat flux variations we find in the periodic regime are very small.

For $\sigma=1$, Eq. (5.9) yields a threshold of 1.24 at infinite wavelength. For $a_2=0.1$ and $a_1=0.72$, the threshold is about 1.25. At $r=1.4$, the modes associated with two wavelengths are large. The motion is periodic. This periodicity can be seen in the graph of $\theta_{002}$ versus time in Fig. 3. The variations in the Nusselt number are about 0.2%.

The next set of calculations was done at $r=1.45$. All four sets of modes are comparable in magnitude, and the motion is weakly nonperiodic. This nonperiodicity can be seen in the graph of $\theta_{002}$ versus time in Fig. 4. There is still a mean field for the roll velocity $u_{101}$ at this stress. The heat flux fluctuations are still only about 0.3%. Figures 5 and 6 show the nonperiodicity over longer and shorter time scales.

Somewhere between $r=1.45$ and 1.50, the mean field in $u_{101}$ drops discontinuously to zero. At $r=1.50$, $u_{101}$ has no mean field and the mode switches sign periodically. The motion at this stress is periodic. This periodicity can be seen in Fig. 7. The variations in the heat flux are about 0.02%. The modes involved with two different wavelengths in the $y$ direction dominate the motion. The reason for the return to periodicity at $r=1.5$ is that the mean field, which contributes to the growth of the perturbations at higher wave numbers at $r=1.45$, disappears. A competition between time scales now determines whether higher-lying modes can produce a bifurcation or not. It is necessary to go to higher stresses before the additional degrees of freedom can become unstable.

At $r=1.55$, the motion is still periodic, as can be seen in Fig. 8. Three wavelengths now dominate the dynamics. The heat-flux variations are about 0.03%.

Finally, at $r=1.6$, the modes associated with all four wavelengths have comparable magnitudes. Figure 9 shows that the motion is strongly nonperiodic. The rms value of the fluctuations in Nusselt number is 1.4%, in reasonable agreement with the 1% value measured by Ahlers. The time scales

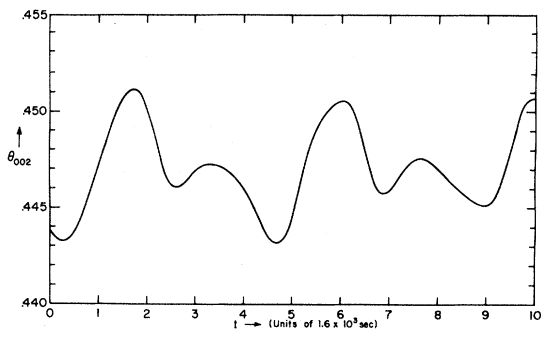


FIG. 6. Expanded view of $\theta_{002}$ vs $t$ for $r=1.45$, 4 wavelengths.

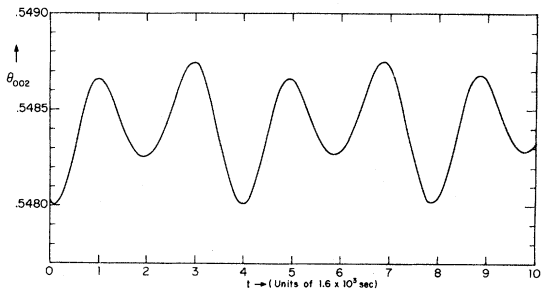


FIG. 8. $\theta_{002}$ vs $t$ for $r=1.55$, 4 wavelengths.

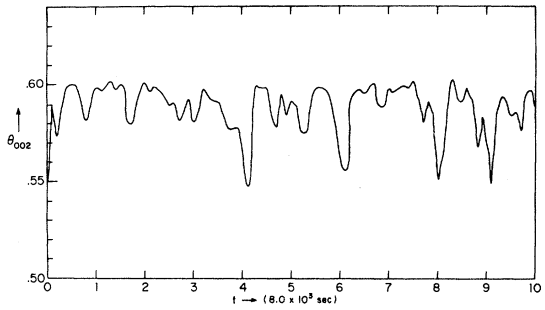


FIG. 9. $\theta_{002}$ vs $t$ for $r=1.6$, 4 wavelengths.

do not agree as well. In the 39-mode system the time scale is about two or three times that found by Ahlers and shown for comparison in Fig. 10.

The time correlation function and power spectrum of the fluctuations in Nusselt number for $r=1.6$ are shown in Figs. 11 and 12. The statistics on these curves are poor, and they should only be used to gain a rough idea of the magnitude and coherence length of the fluctuations. The values for the quantities are compatible with visual inspection of the fluctuations themselves. Figure 13 shows the actual power spectrum which Ahlers measured.

In order to check the idea that four degrees of freedom are necessary to produce nonperiodicity, calculations were performed with the $(4k_y)$ mode omitted from the system. As shown in Fig. 14, the motion was then periodic for $r=1.6$. To see whether nonperiodicity might set in at higher stresses, calculations were also performed at $r=2$ and $r=20$. Figures 15–17 show that the three-mode motion remained periodic at these Rayleigh numbers.

The above calculations suggest that the Ruelle-Takens picture of the transition to nonperiodicity is correct for low-Prandtl-number convection. Let us now turn to some of the experimental evidence. The experiments of Willis and Deardorff[4] show that there are regimes of periodic and nonperiodic flow in low-Prandtl-number convection.

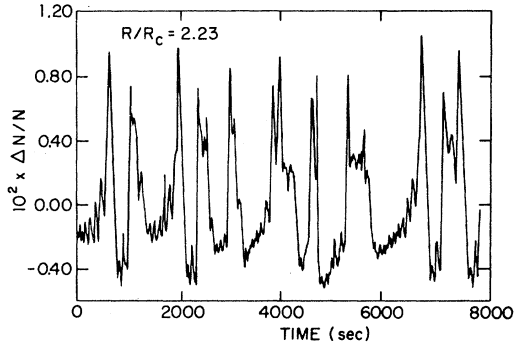


FIG. 10. $\Delta N$ vs $t$ for Ahlers's experiments ($r=2.23$).

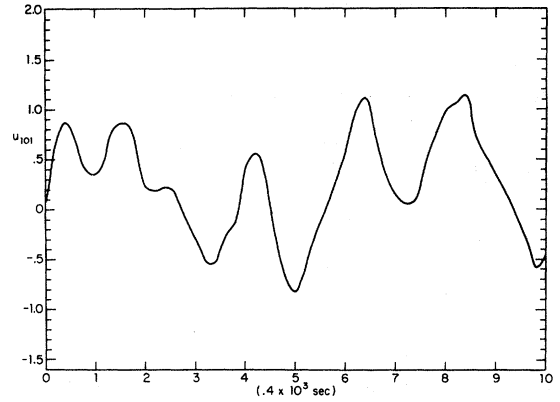


FIG. 11. $u_{101}$ vs $t$ for $r=1.6$, 4 wavelengths.

In Couette flow, the experiments of Coles[3] show that there is a periodic regime. The Taylor cells have a wavy appearance similar to that of the convection cells in their periodic regime. Figure 19 of Coles's paper shows that the appearance of unsteady flow is accompanied by the growth of spatial harmonics. Figure 20 of Coles's paper also illustrates this point.

The experiments of Klebanoff, Tidstrom, and Sargent[6] on the transition to turbulence in a boundary layer also add support to the Ruelle-Takens picture. In these experiments, a two-dimensional Tollmien-Schlichting wave was excited in a boundary layer flow over a flat steel plate. This wave amplified as it propagated downstream until it became three dimensional at a certain point. The three dimensionality consisted of a periodic spanwise variation superimposed on the wave form. The wave then became nonlinear in a very short distance. A theoretical explanation of the subsequent behavior has been given by Landahl.[22] There is a nonlinear rectification mechanism which tends to clip off the positive parts of the waves, leaving negative spikes. At distances close to the point

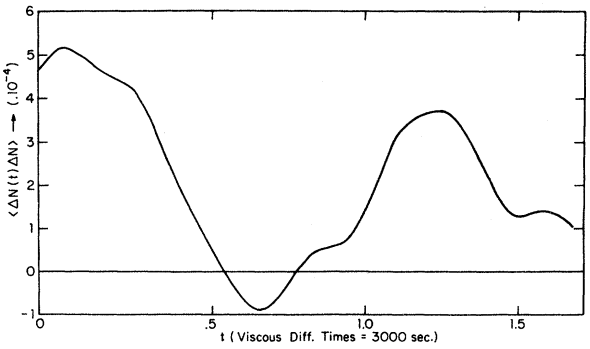


FIG. 12. $\langle \Delta N(t) \Delta N \rangle$ vs $t$ for $r=1.6$, 4 wavelengths.

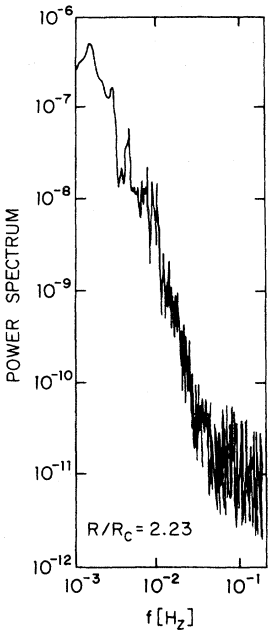


FIG. 13. Ahlers's power spectrum for $r=2.23$.

of breakdown, there is a regime where there is one spike per cycle. As the wave passes further downstream, it enters regions of higher effective Reynolds number. Eventually, a region is reached where there are two spikes per cycle, and, further on, three and four. Figure 21 of Klebanoff, Tidstrom, and Sargent[6] shows that, after four spikes have appeared, the motion becomes nonperiodic. Thus it appears that nonperiodicity develops after the fourth bifurcation.

The experiments of Miksad[5] on transition to turbulence in free shear layers are not as helpful as the boundary-layer experiments. In these experiments, a shear layer was formed by combining two fan-generated winds at the end of a splitter

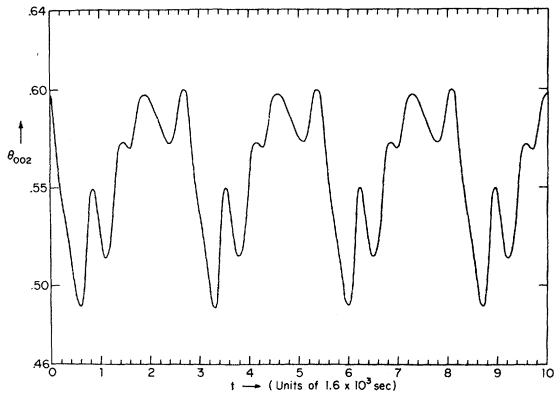


FIG. 14. $\theta_{002}$ vs $t$ for $r=1.6$, 3 wavelengths.

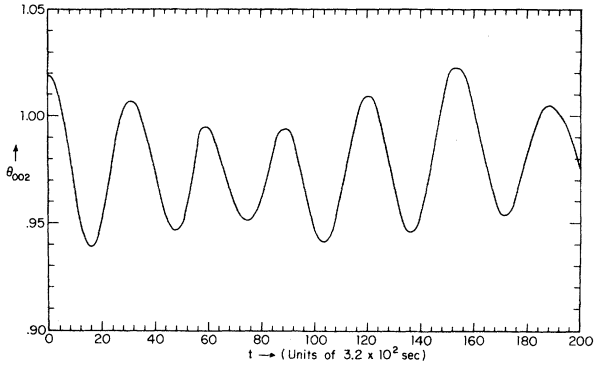


FIG. 15. $\theta_{002}$ vs $t$ for $r=2.0$, 3 wavelengths.

plate. Miksad induced a well-defined frequency in the shear layer by means of a loud speaker. Figure 8 of Miksad's paper shows that there is a regime where there are well-defined spikes in the frequency spectrum. A transition to a continuous spectrum is found, but it is not clear how many bifurcations have occurred since the data at higher frequencies are not displayed.

Feynman[2] gives an account of the transition to turbulence in flow past a cylinder. At low speeds, there is a vortex street behind the cylinder. The velocity at a given point in this vortex street is a periodic function of time. Feynman points out that the appearance of unsteadiness is accompanied by the appearance of spatial harmonics. Unfortunately, the measurements are not sufficiently quantitative to indicate the number of bifurcations that have occurred.

Finally, support for the Ruelle-Takens picture is found in the calculations of Lorenz[7] for a two-layer twelve-mode model of the earth's atmosphere. In these calculations, Lorenz could control the number of degrees of freedom involved in the dynamics. In one set of calculations, he allowed

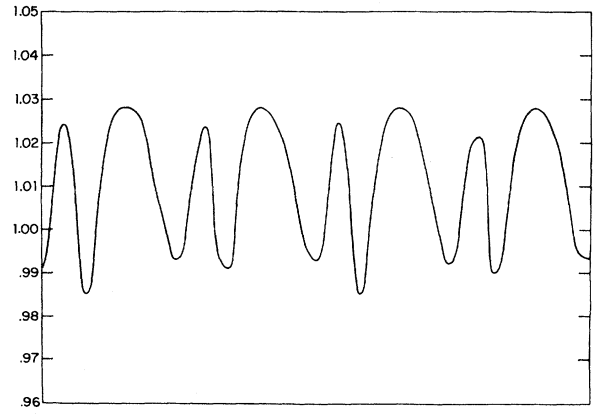


FIG. 16. Maxima of $\theta_{002}$ for $r=2.0$, 3 wavelengths.

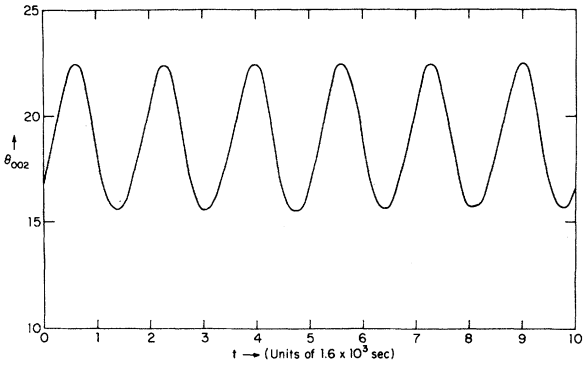


FIG. 17. $\theta_{002}$ vs $t$ for $r=20$, 3 wavelengths.

for two degrees of freedom and obtained a doubly periodic motion. In the next set, he allowed for three degrees of freedom and obtained a triply periodic motion. Finally, when Lorenz allowed for the fourth degree of freedom, he obtained a nonperiodic motion in which correlation functions of the dynamical variable phase mix to zero as their time differences go to infinity.

## VI. SUMMARY AND CONCLUSIONS

The basic goal of this paper has been to present a unified picture of the transition to turbulence in fluid systems which are subjected to static external forces. The Hopf bifurcation theorem plays a central role in this classification. Channel flow, coaxial pipe flow, and the Lorenz model of convection are examples of inverted bifurcation. Inverted bifurcations exhibit a one-parameter family of unstable limit cycles below the linear threshold in stress. Finite amplitude instabilities, hysteresis phenomena, and an abrupt transition to turbulence above the linear threshold are characteristic of the flows in this category. The Lorenz model was discussed in Sec. IV.

Low-Prandtl-number convection, Couette flow, free shear layers, boundary layers, and flows past obstacles exhibit normal bifurcation. Normal bifurcations exhibit a one-parameter family of stable limit cycles above the linear threshold. A picture of the transition to turbulence in such flows, due to Ruelle and Takens, was discussed in Sec. II. This picture was supported by calculations of low-Prandtl-number convection in Sec. V. The available experimental results for the various flows were also discussed. These results appear to support the Ruelle-Takens picture.

It should be remembered that the Ruelle-Takens analysis is based on finite-dimensional phase spaces. They do not consider the possibility of infrared instabilities to a continuum of wave numbers. Preliminary calculations indicate that such instabilities do not occur in low-Prandtl-number convection for the Rayleigh numbers of interest in this paper.

---

*Supported in part by National Science Foundation Grant No. GP06504.

†Present address: Dept. of Physics, Clarkson College, Potsdam, N.Y.

[1]L. D. Landau and E. M. Lifshitz, *Fluid Mechanics* (Pergamon, New York, 1959).

[2]R. P. Feynman, R. B. Leighton, and M. Sands, *The Feynman Lectures on Physics* (Addison-Wesley, Reading, Mass., 1964), Vol. II.

[3]D. Coles, J. Fluid Mech. 21, 385 (1965).

[4]G. E. Willis and J. W. Deardorff, J. Fluid Mech. 44, 661 (1970).

[5]R. W. Miksad, J. Fluid Mech. 56, 4 (1972); 56, 695 (1972).

[6]P. S. Klebanoff, K. D. Tidstrom, and L. M. Sargent, J. Fluid Mech. 12, 1 (1962).

[7]E. N. Lorenz, in Proceedings of the International Symposium Numerical Weather Prediction, Tokyo, 1962 (unpublished), pp. 629-635.

[8]D. Ruelle and F. Takens, Commun. Math. Phys. 20, 167 (1971).

[9]D. D. Joseph and D. H. Sattinger, Arch. Ration. Mech. Anal. 45, 79 (1972); T. S. Chen and D. D. Joseph, J. Fluid Mech. 58, 2, 337 (1973).

[10]S. Smale, Bull. Am. Math. Soc. 73, 747 (1967).

[11]J. A. Whitehead, Am. Sci. 59, 444 (1971).

[12]Lord Rayleigh, Philos. Mag. 32, 529 (1916).

[13]F. H. Busse, J. Fluid Mech. 52, 1, 97 (1972).

[14]R. Krishnamurti, J. Fluid Mech. 42, 309 (1970).

[15]R. Krishnamurti, J. Fluid Mech. 60, 285 (1973).

[16]H. T. Rossby, J. Fluid Mech. 36, 309 (1969).

[17]D. A. Gough, E. A. Spiegel, and J. Toomre (unpublished).

[18]A. S. Monin and A. M. Yaglom, *Statistical Fluid Mechanics* (MIT, Cambridge, Mass., 1971), Vol. I.

[19]E. N. Lorenz, J. Atmos. Sci. 20, 130 (1963).

[20]G. E. Willis and J. W. Deardorff, J. Fluid Mech. 23, 337 (1965).

[21]G. Ahlers (unpublished). A preliminary report occurs in the Bull. Am. Phys. Soc. 17, 59 (1972).

[22]M. Landahl, J. Fluid Mech. 56, 4, 775 (1972).